INSTITUTE OF PHYSICS PUBLISHING JOURNAL OF PHYSICS B: ATOMIC, MOLECULAR AND OPTICAL PHYSICS

J. Phys. B: At. Mol. Opt. Phys. **39** (2006) 3945–3956 doi:10.1088/0953-4075/39/18/023

(e, 2e) ionization measurements from the $3\sigma_g$ and $2\sigma_u^*$ states of N_2—comparison between experiment and theoretical predictions of the effects of exchange, polarization and interference

Andrew James Murray[1], Martyn J Hussey[1], Junfang Gao[2] and D H Madison[2]

[1] School of Physics and Astronomy, University of Manchester, Manchester M13 9PL, UK
[2] Department of Physics, University of Missouri-Rolla, Rolla, MO 65409, USA

Received 27 June 2006, in final form 7 August 2006
Published 12 September 2006
Online at stacks.iop.org/JPhysB/39/3945

Abstract

Gao *et al* (2005 *Phys. Rev.* A **72** 032721) have predicted a Young's type interference effect in the fully differential cross sections for ionization of the $3\sigma_g$ state of N_2 for highly asymmetric collisions with one electron detector fixed at very small scattering angles (1° or 10°). The purpose of this work was to look for this interference effect at a larger scattering angle. (e, 2e) ionization measurements have been conducted from the $3\sigma_g$ and $2\sigma_u^*$ states of N_2 in a coplanar asymmetric geometry, where one electron emerges in the forward direction and the correlated electron is measured as a function of scattering angle. Both final-state electrons have an energy of 30 eV, and the forward scattering angle was $\theta_a = 22°$ relative to the incident beam direction. The theoretical prediction is that there should be a strong interference peak near 180°. The measurements were carried out from the $3\sigma_g$ state over a range of scattering angles from $\theta_b \sim 10°$ to $\theta_b \sim 170°$ using a magnetic angle changing spectrometer. The present experimental results for $3\sigma_g$ find a normal binary peak plus another peak at back angles in the vicinity of 180°. Consequently, this work supports the possibility of a strong Young's type interference effect for small fixed scattering angles.

(Some figures in this article are in colour only in the electronic version)

1. Introduction

Considerable interest has been generated recently in the possibility of measuring the effects of two-centre interferences in the charged particle impact ionization of diatomic molecules. To date, most of the work has concentrated on ionization by heavy particles [1–4]. If diatomic molecules exhibit double slit interference effects, the important question concerns how these

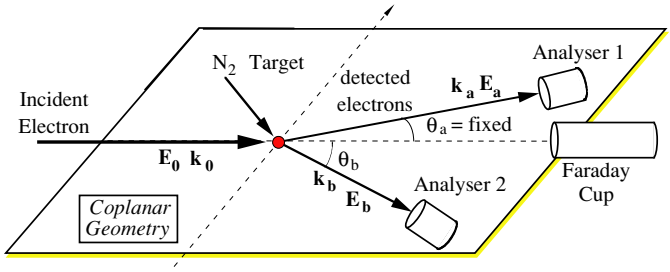

Figure 1. The coplanar asymmetric geometry, where one of the analyser angles is fixed in space.

effects can be observed. Most of the work so far has concentrated on comparing ionization cross sections for diatomic molecules and comparable atoms. For example, it has been shown [5] that the ratio of the FDCS (fully differential cross sections) for molecular hydrogen divided by the cross section for two distinguishable hydrogen atoms is related to the sinc function whose argument is qR (momentum transfer times internuclear separation). If one integrates over θ (projectile scattering angle), the oscillatory nature of the sinc function translates into an oscillatory energy dependence for the double differential cross sections. The search for interference effects in heavy particle scattering has concentrated on looking for these energy-dependent oscillations in the DDCS (doubly differential cross sections) [6–8]. If interference effects can be seen in the DDCS, then they should be more easily observable in the FDCS. For the FDCS, the sinc function modifies the shape of the angular distributions. The typical coplanar asymmetric FDCS contains a large binary peak and a smaller recoil peak and the (recoil peak)/(binary peak) ratio is one way to characterize the shape of the distribution. Consequently, if interference effects are present, this ratio should be different for molecular hydrogen as compared to two distinguishable hydrogen atoms. Although Murray [9] found no evidence for interference effects in the FDCS for electron-impact ionization of H_2 for coplanar symmetric scattering, Milne-Brownlie *et al* [10] recently found a strong indication for interference effects in electron-impact ionization of H_2 for coplanar asymmetric scattering.

If interference effects are observable in the FDCS for electron H_2 scattering, they might be even more pronounced for heavier diatomic molecules. Recently, Gao *et al* [11] predicted that large Young's type interference effects should be observable for electron ionization of the $3\sigma_g$ state of N_2. The M3DW (molecular three-body distorted wave) calculations at an incident energy of 75.6 eV predict that large peaks should be observed in the backward scattering direction, these peaks dominating the ionization process. Their results indicate that for a coplanar asymmetric geometry (see figure 1) where one of the electrons leaves the interaction region at a set angle $\theta_a = 1^\circ$ or $\theta_a = 10^\circ$, the cross section is expected to peak at a scattering angle $\theta_b = 180^\circ$, with additional peaks at around $\theta_b = 120^\circ$ and $\theta_b = 240^\circ$. In these calculations, the electrons leave the interaction region with equal energy of 30 eV.

The strong interference effects predicted at this energy should be observable by experiment, although it is very difficult in practice to measure the cross section for such small angles θ_a at these energies. The (e, 2e) spectrometer in Manchester [12, 13] is able to access a wide range of scattering geometries at low energies, and so provides an ideal test bed for a close comparison between theoretical predictions and experimental data. In practice, the spectrometer cannot access scattering geometries below $\theta_a = 22^\circ$, due to problems with the incident electron beam striking the side of the analyser and causing unacceptably high levels of noise on the coincidence signal.

To harmonize the theoretical predictions with the experimental limitations, new calculations have therefore been performed for the same incident energy of 75.6 eV, with

the scattered angle θ_a now set to 22°. This allows a robust comparison between theory and experiment, although this comparison is on a relative scale, as absolute experimental cross sections are not measured. The spectrometer has also been modified to include a magnetic angle changing (MAC) device, so that the cross section can be determined over a wider angular range than is possible directly. Inclusion of the MAC device allowed the cross sections to be determined from θ_b near 0° to $\theta_b \sim 170°$, so that theoretical predictions of peaks at higher angles could be investigated.

This paper is divided into five sections. Following this introduction, the experimental apparatus and the installation and characterization of the MAC device in the (e, 2e) spectrometer are described. The theoretical calculations are then discussed in section 3, and the predicted cross section for $\theta_a = 22°$ is presented using the M3DW approximation. Section 4 compares experimental results to theory for the $3\sigma_g$ state. All data were collected for equal outgoing electron energies of 30 eV. The last section contains conclusions and suggestions for future work in this area.

2. Experimental setup

The (e, 2e) spectrometer at Manchester has been well documented [12–16], and so will only be described briefly here. The apparatus can be fully computer optimized and controlled throughout data collection, so that the analysers and electron gun are maintained at their optimum operating conditions. The spectrometer can access all geometries from the coplanar geometry to the perpendicular plane, although this facility was not used here. The spectrometer is designed to operate at low to intermediate energies, ranging from around 10 eV to 300 eV incident energy, whereas the analysers are capable of operating over a range of energies from ~0.5 eV to around 100 eV, depending on the setting of the input electrostatic lenses.

Modifications have been made to the spectrometer that allow access to higher scattering angles than were possible previously. In particular, the electron gun has been rebuilt so that the maximum backward scattering angles are increased from $\theta_{a,b} = 125°$ to $\theta_{a,b} = 140°$. A further modification has been the inclusion of a vacuum compatible XY-translator to adjust the position of the electron gun accurately [17], together with a permanently mounted laser diode which traces the direction of the incident electron beam through the interaction region. These additions simplify the alignment of the spectrometer over the angular geometry which can be accessed.

The most significant addition for the present work has been the installation of a magnetic angle changing (MAC) device into the spectrometer. This device uses a well-controlled magnetic field to manipulate the direction of the incident and scattered electrons through the interaction region so as to increase the available angles where the cross section can be measured. The MAC device was invented in Manchester and has proven to be a very useful tool for the determination of angular measurements over the full scattering range [18, 19].

In the version adopted here, a twin coil MAC device with a gap spacing of 6.5 mm has been installed into the (e, 2e) spectrometer so that the field in the centre of the coils is non-zero. Figure 2 shows the axial magnetic field from these coils as a function of the radial distance from the interaction region, calculated using the CPO-3D programme [20]. As can be seen, the field peaks at the interaction region and passes through zero at a radial distance of 10 mm before finally decaying to zero at a distance of 25 mm from the interaction region. Since the entrance to the analysers is 35 mm from the interaction region, the MAC device ensures that the trajectories of the electrons remain unaffected by the B-field once the electrons have entered the analyser input lenses.

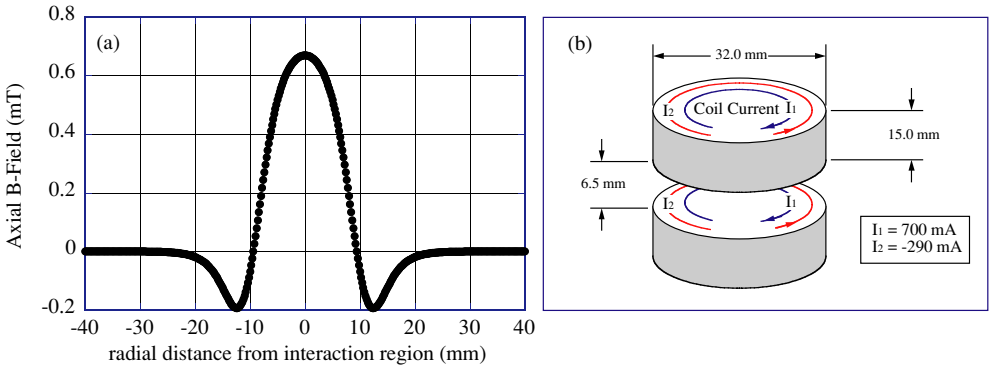

Figure 2. (a) The predicted axial magnetic field from the MAC device, showing the field in the interaction region and at a radial distance from the centre, for a coil current of 700 mA/−290 mA. The field is seen to be zero at $r = 35$ mm, which is the distance to the entrance of the analyser lenses. (b) Representation of the coils, showing the direction of the currents for the inner and outer coils, together with the actual size of the MAC device.

After installation of the MAC device into the (e, 2e) spectrometer, the *B*-field from the coils was measured using a sensitive Bartington magnetometer [21], and this confirmed that this field was zero at the required radial distance. Measurements were conducted for a series of different coil currents to establish the relative currents between the coils so that the field remained zero at the analyser entrance.

To calibrate the relative deflection angle of the electrons which pass through the interaction region between the coils in the MAC device, experiments were performed which measured the elastic cross section from argon at different incident energies. Argon is a useful target for these studies, as deep minima appear in the cross section which can easily be identified. An example of the effects of the MAC device on the argon signal is shown in figure 3 for an incident electron energy of 75.6 eV. Figure 3(a) shows the results from analysers 1 and 2 (see figure 1) when no magnetic field is applied, plotted on a logarithmic scale. A deep minimum is seen at a scattering angle of $63.5^\circ \pm 2^\circ$ at this energy. When a current of 700 mA is passed through the inner coil and –290 mA passed through the outer coil (as set from the field calibration studies), the electrons in each analyser appear to separate in relative angle, as shown in figure 3(b). For analyser 1, the dip moves away to $81^\circ \pm 2^\circ$, whereas for analyser 2 the dip moves closer to $46^\circ \pm 2^\circ$. A second minimum is also seen for this analyser at $116^\circ \pm 2^\circ$, which could not be observed in the direct signal shown in figure 3(a).

The separation occurs since the analysers observe the electrons on opposite sides of the incident beam, and so the resultant force pushes one electron away from the forward direction while moving the second electron towards the forward direction. Since the scattering process that is observed is elastic, the force is equal for both incident and scattered electrons and so the total deflection angle is the same for both ingoing and outgoing electrons.

From these results, the total shift in angle of the electrons passing into the MAC device is seen to be $\sim 17.5^\circ$ for both analysers. This averages to a deflection angle of the 75.6 eV electrons at this MAC current of $2\theta_{\mathrm{defl}}^{75.6\,\mathrm{eV}} = 17.5^\circ \pm 2.8^\circ$ or $\theta_{\mathrm{defl}}^{75.6\,\mathrm{eV}} = 8.8^\circ \pm 1.4^\circ$.

Similar measurements were carried out for a range of incident beam energies from 20 eV to 100 eV, so that a fit to the data as a function of energy could be implemented. The results of this analysis are shown in figure 4, where a simple linear function is fitted to the data which has been constrained to zero at high incident energies. The curve that was adopted

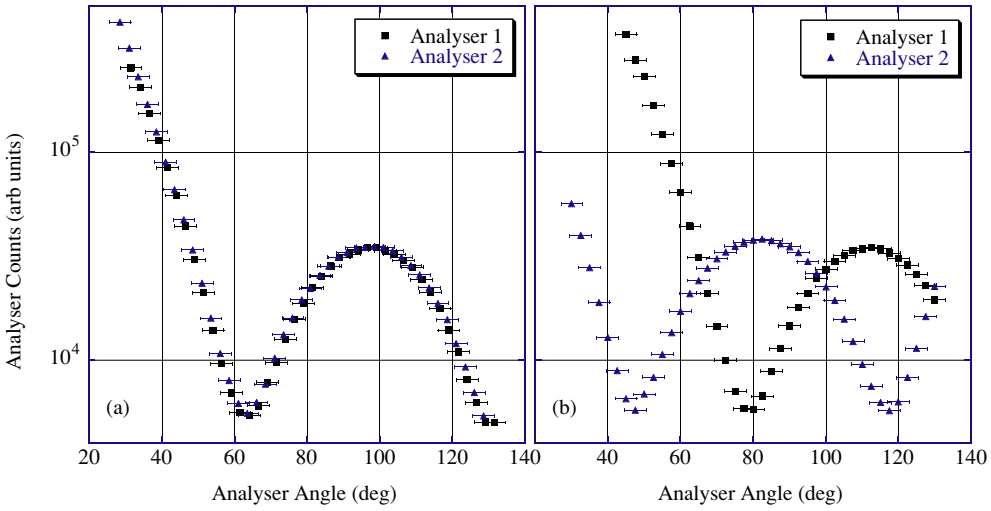

Figure 3. Measurement of the elastic cross section for argon at an incident energy of 75.6 eV, plotted on a logarithmic scale. A deep minimum is seen at $\theta = 63.5^\circ$ which shifts in angle when the field from the MAC device is applied. The relative shift is reversed with respect to the initial direction for each analyser, due to the electrons being detected on opposite sides of the interaction region (see figure 1).

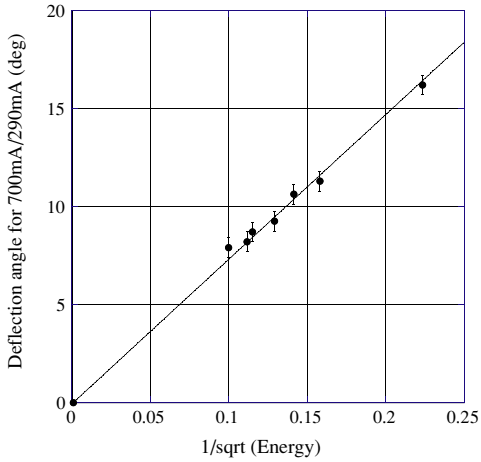

Figure 4. Calibration curve showing the deflection angle as a function of incident energy at a current of 700 mA/−290 mA in the MAC coils. A linear fit has been made to the data. For details, see the text.

is of the form

$$\theta_{\mathrm{defl}}^{E\ (\mathrm{eV})} = \alpha + \frac{\beta}{\sqrt{E\ (\mathrm{eV})}}, \tag{1}$$

where for these MAC currents (700 mA, –290 mA) the constants are given by $\alpha = -0.07 \pm 0.01$ and $\beta = 73.9 \pm 1.3$.

The data presented in figure 4 allow the deflection angle to be determined as a function of energy for this coil current, and so the expected deflection angle for 30 eV electrons is $13.5^\circ \pm 2^\circ$. Further data were taken using differing coil currents to determine the effect of the B-field

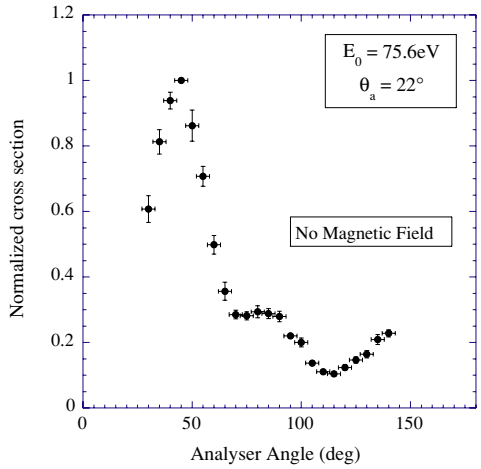

Figure 5. Ionization differential cross section from the $3\sigma_g$ state of N_2, collected without the MAC device operating. The data are normalized to unity at $\theta_b = 45^\circ$. The forward scattering angle is 22° and the incident energy is 75.6 eV. Both outgoing electrons carry 30 eV energy away from the interaction region.

on deflection angle at energies of 75.6 eV and 30 eV, which correspond to the incident and scattered electron energies used in this study. This was carried out to calibrate the MAC device as a function of current, so as to check that the device was operating as expected. The data presented in this paper were taken at operating currents of (700 mA, −290 mA), the scattering angles using the MAC device being matched to those adopted when the coil current was zero, with an angular uncertainty around $\pm 2^\circ$.

3. Experimental results

Three sets of data were collected in these experiments. The first was collected from the $3\sigma_g$ state of N_2 which has an ionization potential of 15.6 eV, without the MAC device in operation. These data were collected with $\theta_a = 22^\circ$ and with θ_b ranging from 30° to 140°, as shown in figure 5. Thirteen sweeps of the detection plane were carried out over this range of angles, the final results being derived by averaging over the full set of data. A distinct forward scatter peak is seen when $\theta_b = 45^\circ$, there is a small peak around $\theta_b = 85^\circ$ and a minimum at $\theta_b = 115^\circ$. The cross section once more increases up to $\theta_b = 140^\circ$, at which point the analyser angle could no longer be increased due to the presence of the electron gun. The uncertainty in the data is taken from the statistical error on the mean, and the data have been normalized to unity at $\theta_b = 45^\circ$.

The second set of data which was taken extended the angular results presented in figure 5 using the MAC *B*-field, as shown in figure 6. Using this technique, the range of angles has been extended from $\theta_b = 10^\circ$ to $\theta_b = 170^\circ$. The data are once more normalized at $\theta_b = 45^\circ$, to allow comparison with figure 5. Again, there is a peak at $\theta_b = 45^\circ$, a second peak at $\theta_b \sim 85^\circ$ and a minimum at $\theta_b \sim 115^\circ$. The results at higher angles now show that a third peak occurs at $\theta_b \sim 160^\circ$, which could not be seen using the conventional (e, 2e) technique. The cross section has a minimum close to zero at $\theta_b \sim 0^\circ$, whereas the cross section at $\theta_b \sim 180^\circ$ is around 40% of the maximum at $\theta_b = 45^\circ$. Unlike coplanar symmetric results, there is no constraint on the cross section that requires it to be zero at $\theta_b = 0^\circ$ and $\theta_b = 180^\circ$.

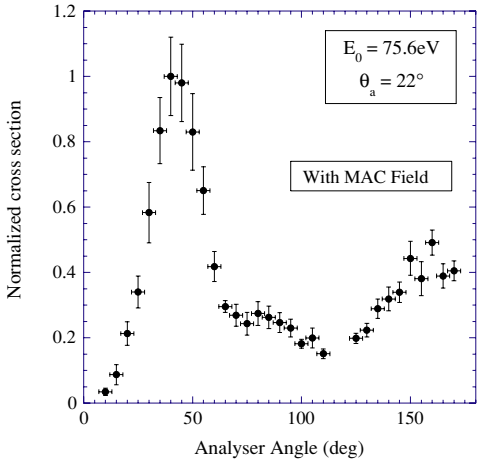

Figure 6. Ionization differential cross section from the $3\sigma_g$ state of N_2, collected with the MAC device operating. The data are again normalized to unity at $\theta_b = 45^\circ$. The forward scattering angle is $22^\circ \pm 2^\circ$ and the incident energy is 75.6 eV. Both outgoing electrons carry 30 eV energy away from the interaction region.

Although the results using the MAC device are very similar to those collected without the B-field present, small differences can be seen. In particular, the minimum at $\theta_b \sim 115^\circ$ is not as deep as when the field is absent, and there is a slight enhancement of the cross section for scattering angles from 125° to 140°. This is thought to be due to the uncertainty in determining the scattering angles which arise when using this device. In particular, small variations in the forward scattering angle θ_a will give rise to changes in the measured cross section, and it is likely that this variation contributes to the differences that are observed. The poorer statistical uncertainty in the data presented in figure 6 is due to a restricted set of results, which arose since one of the analyser electron detectors failed during data collection.

The results for the $3\sigma_g$ state of N_2 can be compared to results from the $2\sigma_u^*$ state at the same collection energy $E_a = E_b = 30$ eV, as presented in figure 7. In this case, the ionization energy is 18.7 eV, and so the electron gun was set to $E_{inc} = 78.7$ eV during data collection. This state is also of σ character, however in contrast to the $3\sigma_g$ valence state, it is a repulsive state with no minimum in the potential energy curve. As such, the electrons in this state are expected to be more confined to a region around the ionic core of the molecule, and so should present a better target for future two-centre interference studies.

The experimental data from this state are however similar to those from the $3\sigma_g$ state, as shown in figure 7. There is again a maximum in the cross section at forward angles, however this now occurs at $\theta_b \sim 60^\circ$. The peak is broader than for the $3\sigma_g$ state, and no secondary peak is observed. The minimum in the cross section now occurs at $\theta_b \sim 90^\circ$, and the cross section once more rises beyond this angle where it is seen to plateau at $\theta_b \sim 120^\circ$. No data were taken from this state using the MAC device due to the failure of the analyser detector, as mentioned above. There is no evidence of large two-centre interference structures in these data.

4. Theory

The molecular three-body distorted wave (M3DW) approximation has been presented in previous publications [22–26], so only a brief overview will be presented here. The M3DW

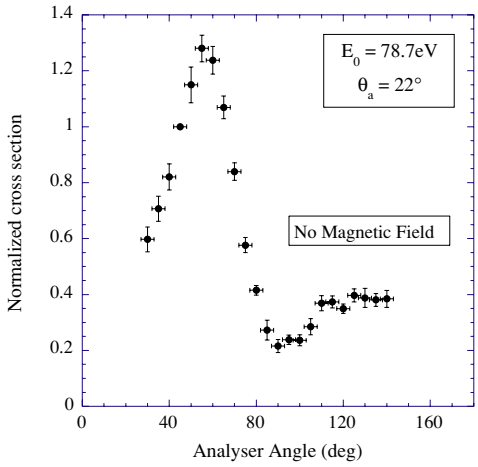

Figure 7. Ionization differential cross section from the $2\sigma_u$ repulsive state of N_2, collected without the MAC device operating. The data are normalized to unity at $\theta_b = 45^\circ$. The forward scattering angle is 22° and the incident energy is 78.7 eV. Both outgoing electrons carry 30 eV energy away from the interaction region.

FDCS (fully differential cross section) is given by

$$\frac{d^5\sigma}{d\Omega_a d\Omega_b dE_b} = \frac{1}{(2\pi)^5}\frac{k_a k_b}{k_i}(|T_{dir}|^2 + |T_{exch}|^2 + |T_{dir} - T_{exch}|^2), \tag{2}$$

where $\vec{k}_i$ is the initial-state wave vector, $\vec{k}_a$ ($\vec{k}_b$) is the wave vector for the scattered (ejected) electron, and the direct and exchange amplitudes are T_{dir} and T_{exch}, respectively:

$$T_{dir} = \langle \chi_a^-(\vec{k}_a, \mathbf{r}_1)\chi_b^-(\vec{k}_b, \mathbf{r}_2)C_{scat-eject}(r_{12})|V - U_i|\phi_j^{OA}(\mathbf{r}_2)\chi_i^+(\vec{k}_i, \mathbf{r}_1)\rangle, \tag{3}$$

$$T_{exc} = \langle \chi_a^-(\vec{k}_a, \mathbf{r}_2)\chi_b^-(\vec{k}_b, \mathbf{r}_1)C_{scat-eject}(r_{12})|V - U_i|\phi_j^{OA}(\mathbf{r}_2)\chi_i^+(\vec{k}_i, \mathbf{r}_1)\rangle. \tag{4}$$

In equations (3) and (4), $\mathbf{r}_1$ ($\mathbf{r}_2$) are the coordinates of the incident (bound) electron, χ_i, χ_a and χ_b are the distorted waves for the incident, scattered and ejected electrons, respectively, ϕ_j^{OA} is the orientation-averaged molecular orbital (OAMO) [25] for the initial bound state of the molecule generated from molecular orbitals calculated using GAMESS [27], V is the initial-state interaction between the projectile and the neutral molecule, and U_i is the initial-state spherically symmetric distorting potential which is used to calculate the initial-state distorted wave χ_i. The $C_{scat-eject}$ term is the Coulomb interaction between the scattered projectile and the ejected electron. Since this post-collision interaction (PCI) term is included in the final-state wavefunction, the effects of PCI are included to all orders of perturbation theory.

The molecular distorted waves are calculated using a spherically averaged distorting potential as described in previous works [22–26]. The Schrödinger equation for the incoming electron wavefunction is given by

$$\left(T + U_i - \frac{k_i^2}{2}\right)\chi_i^+(\vec{k}_i, r) = 0, \tag{5}$$

where T is the kinetic energy operator and the '+' superscript on $\chi_i^+(\vec{k}_i, r)$ indicates outgoing wave boundary conditions. The initial-state distorting potential contains three components $U_i = U_S + U_E + U_P$, where U_S is the initial-state spherically symmetric static potential, U_E

is the exchange potential which treats the effect of the continuum electron exchanging with the passive bound electrons in the molecule and U_P is the polarization potential. For the exchange potential U_E, we use the Furness–McCarthy [28] approximation which has been widely used for atomic scattering. In this approximation, the exchange potential U_E depends on the molecular charge density

$$U_E = -\tfrac{1}{2}\left\{\left(k_i^2 - U_S\right) - \sqrt{\left(k_i^2 - U_S\right)^2 + 2\rho_S(r)}\right\}. \tag{6}$$

Here $\rho_S(r)$ is the spherically averaged molecular electronic charge density. The radial charge density is defined such that the integral over r yields the number of electrons in the molecule. For the polarization potential U_P, we use a phenomenological approximation

$$U_P = -\frac{\alpha_0}{2r^4}\left\{1 - \exp\left[-\left(\frac{r}{a}\right)^6\right]\right\}, \tag{7}$$

where α_0 is the dipole polarizability and a is an adjustable parameter that acts as a cut-off radius for the polarization potential. The dipole polarizability α_0 is 11.744 au for N_2 and admittedly a better approximation for polarization is also desirable [29]. However, this potential has been often used for molecular scattering and is known to provide at least the qualitative effects of polarization.

The two final channel distorted waves are obtained from a Schrödinger equation similar to equation (5):

$$\left(T + U_i + U_E + U_P - \frac{k_{a(b)}^2}{2}\right)\chi_{a(b)}^-(\vec{k}_{a(b)}, r) = 0. \tag{8}$$

Here U_i is the spherically symmetric static distorting potential for the molecular ion which is calculated using the same procedure as U_S except that the active electron is removed from the charge distribution. The '–' superscript indicates incoming wave boundary conditions.

5. Comparison between theory and experiment

For the standard coplanar symmetric scattering geometry where both final-state electrons have the same energy and are observed at the same angle on opposite sides of the incident beam direction, the direct and exchange amplitudes are identical, so only one amplitude needs to be evaluated. This is not the case for the present experiment since the equal energy electrons are observed at different angles. Consequently, it is of interest to examine the importance of the exchange amplitude. Figure 8 compares experimental and theoretical results for 75.6 eV electron-impact ionization of the $3\sigma_g$ state of N_2 for the case of both final-state electrons having an energy of 30 eV, one of them being observed at a fixed scattering angle of 22° and the second electron being detected on the opposite side of the beam direction over a wide range of angles. All the theoretical results are normalized to experiment at the binary peak ($\theta_a \sim 45°$). In the top part of the figure, only the direct amplitude is used in the M3DW theoretical calculation and in the bottom part of the figure the M3DW results include both the direct and exchange amplitudes. Note that there are two different exchange effects included in the M3DW calculation. The exchange amplitude T_{exc} contains the effect of exchange between the two final-state continuum electrons while the Furness–McCarthy exchange potential U_E contains the effect of exchange between a continuum and a bound electron. Here we are examining the importance of exchange between the two final-state continuum electrons. Although exchange between the two outgoing electrons does not change the overall pattern of the FDCS very much, it does change the relative magnitudes of the peaks and valleys which is particularly

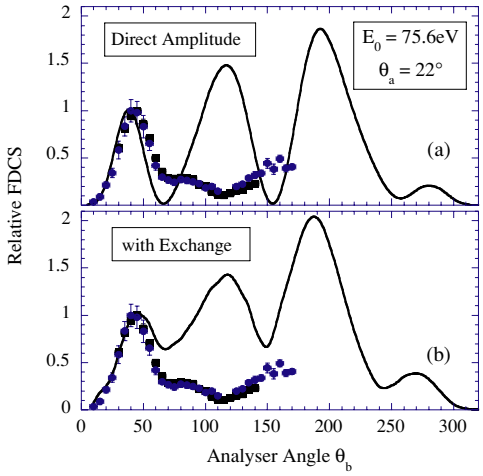

Figure 8. Experimental and theoretical results for 75.6 eV electron-impact ionization of the $3\sigma_g$ state of N_2. Each final-state electron has an energy of 30 eV. One electron is observed at 22° and the second electron is detected at angle θ_b on the opposite side of the beam direction. All theoretical results are normalized to experiment at the binary peak. In (a), only the direct amplitude is used in the M3DW calculation and in (b) the M3DW results include both the direct and exchange amplitudes.

evident for angles of $\theta_b = 65°$ and $\theta_b = 150°$. It is clear that the exchange amplitude cannot be neglected for these kinematics.

For highly asymmetric collisions (i.e. $\theta_a = 1°$ or 10°), Gao *et al* [11] predicted a large interference peak near 180° and a couple of sideband peaks around 80° and 120°. The present M3DW results still contain the large interference peak near 180°. However, the two small interference sidebands found for highly asymmetric collisions are now greatly enhanced and the first one has evolved into the binary peak. The experimental data show no indication of the predicted second peak near 120°.

It is known that the polarization potential can play an important role in low-energy electron-impact collisions [22, 24, 25, 30]. Figure 9 shows the results of using the phenomenological polarization potential of equation (7) for three different cut-off parameters. Both the direct and exchange amplitudes were used in this calculation.

Comparing figures 8 and 9, it is seen that the agreement between experiment and theory is much improved by including the polarization potential. Again the theoretical results are normalized to unity at the experimental binary peak. For a cut-off parameter of $1.25a_0$, the agreement with experimental data is excellent out to about 100°. Since the internuclei distance of N_2 is $R = 2.07a_0$ and the origin of our coordinate system is at the centre of mass, the minimum cut-off parameter we tried was $a = 1.0a_0$, since this corresponds to the radius of the nuclei. It is seen that the polarization potential greatly reduces the relative sizes of the predicted peaks at larger angles as compared to the binary peak. For the smaller cut-off parameters, the second peak near 130° becomes much less pronounced and there is an overall qualitative agreement with experiment for $a = 1.0a_0$. The remnant of the large back angle interference peak predicted for highly asymmetric collisions is still present at about 185° and, although the experimental data do not cover the range of the peak, it is possible that there will be a peak in the data somewhere in that angular range. Since a peak near 180° would not be attributed to a recoil peak, the present measurements are at least consistent with the possibility

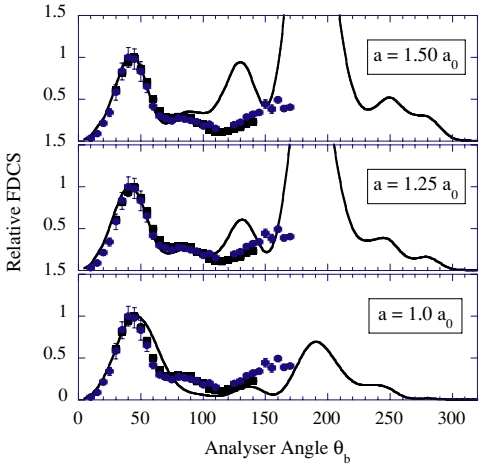

Figure 9. Same as figure 8 except that the theoretical results are for different values of the polarization potential cut-off parameter. Both the direct and exchange amplitudes are used in the M3DW calculations.

of a Young's type interference peak in this angular range. In the simple model proposed by Gao *et al* [11], the interference peak near 180° was attributed to the active electron scattering from the two nuclei and the secondary peak near 130° was attributed to a secondary sideband. Since the interference pattern results from the nuclei and not the molecular electrons, one would expect that the polarization potential should affect the magnitude but not the location of the peaks and this is what is found. However, since the magnitudes of the peaks are very sensitive to the polarization potential, a calculation with an improved potential is obviously highly desirable.

Comparison with the experimental results from the $2\sigma_u^*$ state (figure 7) was not attempted at this time, since it was not considered that the angle averaging procedure adopted in the present theory would be sufficiently accurate for this state.

6. Conclusions

Gao *et al* [11] predicted a strong Young's type interference effect for ionization of the $3\sigma_g$ state of N_2 for highly asymmetric collisions with one electron detector fixed at small scattering angles (1° or 10°). The purpose of this work was to look for this interference effect at a larger scattering angle of 22°. For small scattering angles, it was predicted that there would be a large interference peak near 180°. The present experimental results find a normal binary peak plus a smaller back angle peak in the vicinity of 180°. When polarization is included in the M3DW calculation, the magnitude of the interference peak near 180° is greatly reduced to approximately the size of the measured cross section. Consequently, this work supports the possibility of a strong Young's type interference effect for small fixed scattering angles. Although the present M3DW results are in qualitative agreement with experiment for the smallest cut-off parameters for the polarization potential, a calculation with an improved polarization potential is highly desirable.

As more data on the ionization of molecules become available, it is clear that significant improvements must be made to both experiment and theory to better understand this important

ionization process. Deficiencies in the experiment include the use of rotationally hot molecules and the lack of pre-alignment of the molecular axis prior to ionization taking place. It is possible to perform experiments using supersonically cooled molecules which are all in the ground rotational state ($J = 0$), however it is more difficult to align and orient the molecules prior to ionization. This has been achieved for polar molecules [31] using high-power laser radiation coupled to electrostatic fields or by using hexapole fields [32], however such approaches have not as yet been used in (e, 2e) ionization studies. Different methods are currently being considered for new experiments at Manchester.

Acknowledgments

We would like to thank Alan Venables and Dave Coleman for continued technical support at Manchester. We would also like to thank the Engineering and Physical Science Research Council for providing one of us (MH) with a postdoctoral research associateship during this period. JG and DHM would like to acknowledge the support of the USA NSF under grant PHY-0456528

References

[1] Stolterfoht N *et al* 2001 *Phys. Rev. Lett.* **87** 023201
[2] Stolterfoht N *et al* 2003 *Phys. Rev.* A **67** 030702
[3] Misra D, Kadhane U, Singh Y P, Tribedi L C, Fainstein P D and Richard P 2004 *Phys. Rev. Lett.* **92** 153201
[4] Hossain S, Alnaser A S, Landers A L, Pole D J, Knutson H, Robison A, Stamper B, Stolterfoht N and Tanis J A 2003 *Nucl. Instrum. Methods Phys.* **205** 484–7
[5] Stia C R, Fojón O A, Weck P F, Hanssen J and Rivarola R D 2003 *J. Phys. B: At. Mol. Opt. Phys.* **36** L257-64
[6] Tanis J A, Hossain S, Sulik B and Stolterfoht N 2005 *Phys. Rev. Lett.* **95** 0793011
[7] Hossain S, Landers A L, Stolterfoht N and Tanis J A 2005 *Phys. Rev.* A **72** 10701
[8] Landers A L, Wells E, Osipov T, Carnes K D, Alnaser A S, Tanis J A, McGuire J H, Ben-Itzhak I and Cocke C L 2004 *Phys. Rev.* A **70** 42702
[9] Murray A J 2005 *J. Phys. B: At. Mol. Opt. Phys.* **38** 1999
[10] Milne-Brownlie D S, Foster M, Gao J, Lohmann B and Madison D H 2005 *Phys. Rev. Lett.* **96** 233201
[11] Gao J, Madison D H and Peacher J L 2005 *Phys. Rev.* A **72** 032721
[12] Murray A J, Turton B C H and Read F H 1992 *Rev. Sci. Instrum.* **63** 3346
[13] Murray A J and Read F H 1992 *Phys. Rev. Lett.* **69** 2912
[14] Murray A J 2005 *J. Phys. B: At. Mol. Opt. Phys.* **38** 1999
[15] Murray A J 2005 *Phys. Rev.* A **72** 062711
[16] Murray A J and Cvejanovic D 2003 *J. Phys. B: At. Mol. Opt. Phys.* **36** 4875
[17] Murray A J 2003 *Meas. Sci. Technol.* **14** N1
[18] Read F H and Channing J M 1996 *Rev. Sci. Instrum.* **67** 2372
[19] Linert I, King G C and Zubek M 2004 *J. Phys. B: At. Mol. Opt. Phys.* **37** 4681
[20] Available from http://www.electronoptics.com
[21] Available from http://www.bartington.com
[22] Gao J, Madison D H and Peacher J L 2006 *J. Phys. B: At. Mol. Opt. Phys.* **39** 1275
[23] Gao J, Madison D H and Peacher J L 2005 *Phys. Rev.* A **72** 032701
[24] Gao J, Madison D H and Peacher J L 2005 *J. Chem. Phys.* **123** 204314
[25] Gao J, Peacher J L and Madison D H 2005 *J. Chem. Phys.* **123** 204302
[26] Gao J, Madison D H, Peacher J L, Murray A and Hussey M 2006 *J. Chem. Phys.* **124** 164306
[27] Schmidt M W *et al* 1993 *J. Comput. Chem.* **14** 1347
[28] Furness J B and McCarthy I E 1973 *J. Phys. B: At. Mol. Phys.* **6** 2280
[29] Feng H, Sun W and Morrison M 2003 *Phys. Rev.* A **68** 062709
[30] Gao J, Madison D H and Peacher J L 2005 *Phys. Rev.* A **72** 020701
[31] Minemoto S, Nanjo H, Tanji H, Suzuki T and Sakai H 2003 *J. Chem. Phys.* **118** 4052
[32] Volkmer M, Meier C, Lieschke J, Mihill A, Fink M and Bowering N 1996 *Phys. Rev.* A **53** 1457